Dependence of the Electrochemical and Passive Behavior of the Lead-Acid Battery Positive Grid on Electrode Surface Roughness

Davood Nakhaie,[‡,*,**] Iman Taji,[*] Mohammad Hadi Moayed,[*] and Edouard Asselin[**]

ABSTRACT

The corrosion resistance of the positive grid alloy plays an important role on the performance and service life of lead-acid batteries. There are many parameters influencing the corrosion behavior of the grid alloy. Grid surface roughness, which is of importance from a manufacturing point of view, is a parameter that has received rather less attention. In the present study, the dependence of the electrochemical and the passive behavior of the positive grid alloy on electrode surface roughness was investigated. Cyclic voltammetry, potentiodynamic polarization, galvanostatic polarization, electrochemical impedance spectroscopy, and Mott-Schottky analysis were used to evaluate the influence of surface roughness on the electrochemical properties of the grid alloy. The results indicated that increasing the surface roughness hindered formation of the passive film and increased the corrosion resistance of the lead alloy electrode. Moreover, it was found that the donor density of the passive film is proportional to the surface roughness.

KEY WORDS: lead-acid battery positive grid, n-type semiconductor, passivity, surface preparation, surface roughness, sulfuric acid

INTRODUCTION

Pb-Ca alloys are widely used as a grid alloy in lead-acid batteries. A high overpotential for oxygen and hydrogen evolution reactions on the Pb-Ca alloys compared to Pb-Sb alloys has made them an excellent choice for maintenance-free batteries. However, premature capacity loss, resulting from the formation of a high-impedance oxide at the interface of the grid/active materials, is the main failure factor in batteries manufactured with Pb-Ca alloys.[1-3] Extensive efforts have been made to overcome this. Modifying the grid alloy chemical composition by using alloying elements is a common method to decelerate the grid growth.[4-5] Alloying elements, such as Sn, Ba, and Ag have been successfully used.[6-11] Other elements, such as Ce, Sm, and Y exhibit potential advantages, however, increase the production costs.[12-14]

Alloy composition,[6-7] grid design,[15] battery temperature,[16] and potential for the positive plate[17] are the most important parameters affecting the corrosion behavior of the positive grid alloy. The positive electrode in lead acid batteries typically experiences a potential range from 1,000 mV_{SCE} to 2,000 mV_{SCE}.[18] A high overpotential can enhance the grid corrosion and consequently the failure of the battery. Despite these factors, there are some other manufacturing parameters, such as process control and grid manufacturing route, that influence grid corrosion resistance. It is well known that to improve the battery service life, careful process control is necessary.[18] Furthermore, it has been found that grids produced with different manufacturing processes, e.g., gravity casting and

Submitted for publication: June 6, 2016. Revised and accepted: July 13, 2017. Preprint available online: July 13, 2017, http://dx.doi.org/10.5006/2160.

‡ Corresponding author. E-mail: davood.nakhaie@mtrl.ubc.ca.
* Metallurgical and Materials Engineering Department, Faculty of Engineering, Ferdowsi University of Mashhad, P.O. Box 91775-1111, Iran.
** Department of Materials Engineering, The University of British Columbia, 6350 Stores Road, Vancouver, BC Canada V6T 1Z4.

ISSN 0010-9312 (print), 1938-159X (online)

metal expanding, behave differently. The microstructure, yield and ultimate strength, corrosion resistance, and gassing behavior of lead alloys closely depend on grid production techniques.[19] Therefore, from a practical point of view, it is important to control the manufacturing process in order to extend the battery service life as well as its performance.

The battery grid, which is an absorbent for mechanical stresses and a precursor of the active materials, is responsible for current distribution through the plate. Therefore, the adhesion of the active materials to the grid is of importance. It has been proposed that a jagged grid surface, resulting from occurrence of corrosion at the grain and sub-grain boundaries, may promote the adhesion of the active materials to the grid.[20] Consequently, the grid surface roughness plays an important role on the adhesion of the active materials. One manufacturing variation for grid production is the surface roughness. Even though the rolling and expansion technology fashions grids with smoother surfaces; the surface roughness of grids produced by the gravity casting method depends on the mold quality. It has been shown that the surface roughness influences the critical pitting temperature[21] and metastable pitting of stainless steels,[22-23] and localized corrosion of Al[24] and Mg alloys.[25] In all of these cases, increasing the surface roughness had deteriorative effects on the corrosion resistance of the alloys. To the best of the authors' knowledge, the relationship between the surface roughness and the electrochemical behavior of lead-acid battery grids has not been studied. In the present study, the influence of surface roughness on the corrosion resistance, oxygen, and hydrogen evolution overpotentials and the passive behavior of a Pb-Ca-Sn grid alloy in 4.8 M H_2SO_4 are investigated.

EXPERIMENTAL PROCEDURES

The chemical composition (in wt%) of the lead alloy was Ca 0.09%, Sn 1.23%, and Pb 98.68%. Specimens with surface area of 4.5 cm^2 were mounted in epoxy resin. The exposed surface was then manually ground with SiC grinding paper of different grits with deionized water as a lubricant with different final surface roughness of 60, 600, or 2500 grit finish. The electrode was then rinsed with deionized water and put into use immediately. A conventional three-electrode cell was used with a platinum mesh as counter electrode and a saturated calomel electrode (SCE) as reference electrode. The electrochemical cell was a 250 mL beaker open to the air. All electrochemical experiments performed at 25±1°C in 4.8 M H_2SO_4 solution. For each test a fresh solution was used. Before electrochemical experiments (except for the case of potentiodynamic polarization) the working electrodes were initially reduced potentiostatically at −1,200 mV_{SCE} for 10 min.

In order to characterize the anodic polarization behavior of the lead alloy, potentiodynamic polarization was performed from −150 mV to 2,500 mV with respect to the corrosion potential at a potential scan rate of 30 mV/min. Before polarization, the corrosion potential was monitored for 3,600 s. Cyclic voltammetry (CV) was performed in the potential range from −1,500 mV_{SCE} to 2,500 mV_{SCE} at a scan rate of 1,500 mV/min for one cycle. Also, the CV measurements were repeated from 1,000 mV_{SCE} to 2,500 mV_{SCE} for 50 cycles with the aim of comparing the life cycle of the electrodes. The linear sweep voltammetry (LSV) was performed from 1,200 mV to −1,500 mV at a potential scan rate of 120 mV/min. Before LSV measurement, the electrode was potentiostatically polarized at 1,200 mV_{SCE} for 60 min to grow a passive oxide film.

Capacitance measurements for Mott-Schottky analysis of the passive films formed on the Pb-Ca-Sn alloy were performed after passive film growth at 1,200 mV_{SCE} for 60 min. For each specimen, a small-amplitude sinusoidal voltage perturbation of 10 mV at a frequency of 1,000 Hz was applied. The voltage scan rate of 60 mV/min was sufficiently fast to ensure that the vacancy structure of the passive film was "frozen-in."[26]

In order to measure the true surface area (TS), three samples in cubic form with 60, 600, and 2500 finished grit size were prepared. All dimensions were measured by a micrometer for calculation of apparent surface area (AS). The TS area was measured by Micromeritics® Brunauer-Emmett-Teller (BET) surface area analyzer. The normalization factor (NF) was calculated by dividing these two surface areas:

$$NF = \frac{TS}{AS} \quad (1)$$

The NF for 60, 600, and 2500 grit finish surfaces were 1.4, 1.04, and 1, respectively. These values were used to calculate the current density and impedance values.

RESULTS AND DISCUSSION

Potentiodynamic Polarization

Figure 1 shows the typical potentiodynamic polarization curves for Pb-0.1%Ca-1.2%Sn alloy with different surface roughness obtained in 4.8 M H_2SO_4 at a scan rate of 30 mV/min. As can be seen, in the active dissolution region, which relates to the oxidation of Pb to $PbSO_4$,[27] the anodic Tafel slopes are not influenced by surface condition. Moreover, the corrosion potential remains essentially constant for all specimens. The critical current density increased as the surface roughness increased, which implies that the onset of passivation was hindered on specimens with higher surface roughness. With further increase in the applied potential, the passive film began to break

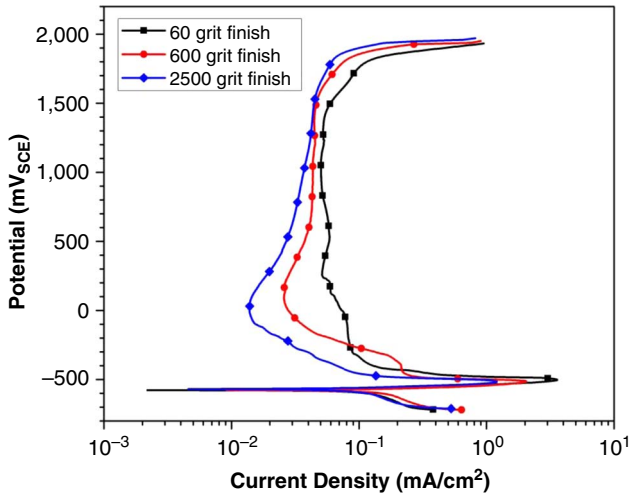

FIGURE 1. *Typical potentiodynamic polarization curves for the lead alloy electrodes with different surface roughness obtained in 4.8 M H_2SO_4 at potential scan rate of 30 mV/min at 25°C. The current density was obtained by considering the normalized surface area for each sample determined from BET analysis.*

down, which corresponds to the oxidation of $PbSO_4$ to PbO_2.

The passive current density of the electrode with the 60 grit surface finish is noticeably greater than that of the electrode with the 600 grit surface finish. The passive layer formed on a Pb electrode has been demonstrated to be a two-layer structure, i.e., Pb/PbO/$PbSO_4$.[28] The instability of the passive film, as assessed by the passive current density, varies correspondingly with the surface condition, i.e., the passive current density increased as surface roughness increased. This suggests that the surface roughness could modify the two-layer structure and make the passive layer more conductive, which has been confirmed by impedance measurements and will be discussed later.

TEM observations have revealed that abrasion and polishing can create an altered surface layer, which contains a heterogeneous microstructure with high density of dislocations, nanosized subgrains, and the redistribution of alloying elements.[24,29] The formation of these microstructural features is believed to be the result of the shear strain generated by contact of solid abrasive particles with the surface.[24] The larger the abrasive particle size of the grinding paper is, the higher the shear plastic deformation. Therefore, the thickness of the altered surface layer increases by increasing surface roughness. Moreover, in lead-calcium-tin alloys, corrosion occurs preferentially alongside the grain boundaries.[18] Consequently, there is a strong possibility that the higher passive current density of the 60 grit finish sample is a result of a higher density of subgrain boundaries on the electrode surface. Similarly, it is likely that approach to the critical current density, which corresponds to the formation of $PbSO_4$, is postponed on rougher surfaces because of higher density of microstructural defects.

Cyclic Voltammetry

Cyclic voltammograms of the lead alloy electrodes in sulfuric acid electrolyte at a scan rate of 600 mV/min are presented in Figure 2(a). The peaks I and II are assigned to oxidation of Pb to $PbSO_4$/PbO and PbO_2, respectively. Peak III relates to the reduction of PbO_2 to $PbSO_4$, and peaks IV and V correspond to the reduction of PbO and $PbSO_4$ to Pb, respectively.[30-32] The potential ranges in the positive and the negative directions are limited by the evolution of oxygen and hydrogen evolution, respectively. The oxidation of tin occurs at the potential for the formation of Pb^{2+}.[33] The values of current density and corresponding potential of all peaks are extracted from the cyclic voltammograms and summarized in Table 1. As can be seen, the intensity of the oxidation peaks (peaks I and II) was increased with increasing surface roughness. This suggests that oxidation of Pb to Pb^{2+} occurred at

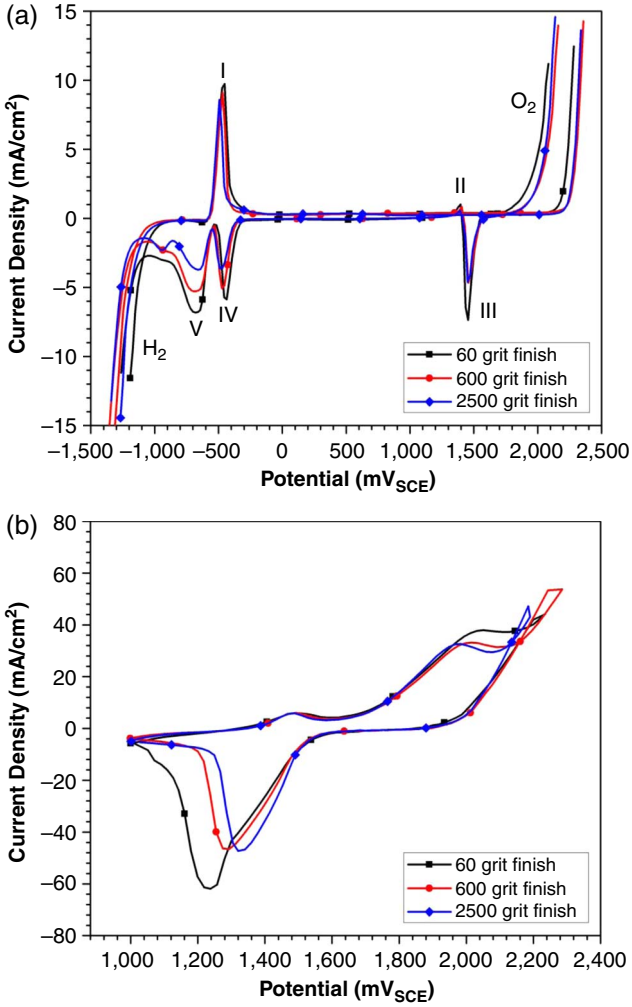

FIGURE 2. *(a) Cyclic voltammograms of the lead alloy electrodes with different surface roughness obtained in 4.8 M H_2SO_4 at potential scan rate of 600 mV/min at 25°C. (b) Cyclic voltammograms obtained after 50 cycles at same conditions as (a). The current density was obtained by considering the normalized surface area for each sample determined from BET analysis.*

TABLE 1

The Values of Current Density and Potential of Oxidation and Reduction Peaks Extracted from the Cyclic Voltammograms of the Lead Alloy Electrodes

		60 Grit Finish	600 Grit Finish	2500 Grit Finish
Peak I	E (mV_{SCE})	–451	–468	–493
	i (mA/cm^2)	9.737	9.101	8.596
Peak II	E (mV_{SCE})	1,396	1,405	1,393
	i (mA/cm^2)	1.017	0.832	0.566
Peak III	E (mV_{SCE})	1,454	1,457	1,451
	i (mA/cm^2)	–7.360	–4.661	–4.604
Peak IV	E (mV_{SCE})	–436	–473	–488
	i (mA/cm^2)	–5.871	–5.056	–3.625
Peak V	E (mV_{SCE})	–681	–696	–661
	i (mA/cm^2)	–6.817	–5.267	–3.7107
Oxygen evolution	E (mV_{SCE})	2,200	2,264	2,254
Hydrogen evolution	E (mV_{SCE})	–1,062	–1,144	–1,115

higher rates on rougher surfaces. Likewise, the current density of reduction peaks III, IV, and V was increased with increasing surface roughness, which implies that the reduction of oxides formed on the electrode with a smooth surface took place more easily compared to a rough surface. On the other hand, the potential of the oxidation reactions shifted to more noble values by increasing the surface roughness.

Figure 2(b) presents the cyclic voltammograms for the lead alloy with different surface finishes after 50 cycles of polarization between 900 mV_{SCE} and 2,250 mV_{SCE} in 4.8 M H_2SO_4 at a scan rate of 600 mV/min. In the positive scanning direction, the oxidation current density of Pb^{2+} to Pb^{4+} for 600 and 2500 grit finish specimens was slightly lower than that of the 60 grit specimen. Moreover, after 50 cycles, the oxygen evolution behavior of the 60 and 2500 grit specimens was almost same, however, the 600 grit finish specimen showed higher overpotential for oxygen evolution.

Compared to the first cycle, the CV behavior showed remarkable changes, regardless of surface finish, i.e., by increasing the number of cycles, current density of peak III increased. This implies that reduction of PbO_2 to $PbSO_4$ took place at higher rates. This behavior was related to the presence of Sn precipitates at the electrode surface.[17] When the oxide layer was sufficiently thick, the oxidation rate decreased, because of the insulating properties of PbO.[34] The oxygen evolution reaction, which proceeds on the positive plates at the end of charge and during overcharge, has an important role on the water loss of a battery.[19-20] Therefore, increasing the oxygen evolution overpotential decreases the water loss. The oxygen evolution overpotential was determined as the potential at which the current density started to abruptly increase in the positive-going sweep. The results summarized in Table 1 show that the 600 grit finish surface possesses the highest oxygen evolution overpotential, while the 60 grit finish electrode shows the lowest value. The overpotential of oxygen evolution on the 2500 grit finish electrode was slightly lower than that of the 600 grit finish sample. As the rate of the oxygen evolution is inversely proportional to the reaction overpotential, one may conclude that a battery produced with grids with 600 grit finish has the lowest tendency for water loss.

Linear Sweep Voltammetry

Figure 3 shows typical voltammograms of the anodic films on the Pb alloy electrodes. The graph was obtained by polarization of the electrode in the cathodic direction after potentiostatic formation of the oxide film at 1,200 mV_{SCE} for 60 min. Peaks 1 and 2 correspond to the reduction of Pb^{2+} oxide to Pb and the reduction of $PbSO_4$ to Pb, respectively.[14] As can be seen in Figure 3, an increase of the surface roughness leads to an increase of the reduction current density of peak 2. The current density of peak 1 remained almost constant for different specimens, while the corresponding potential changed with the surface condition, i.e., the higher the surface roughness, the lower the reduction potential (less positive). By further decreasing potential in the negative direction, the hydrogen evolution reaction occurs (peak 3). The hydrogen evolution overpotential was determined as the potential at which the current density started to sharply decrease in the negative-going sweep. Although the hydrogen evolution overpotential for the 600 and 2500 grit finish electrodes were nearly equal, the specimen with the 60 grit finish surface had a lower overpotential, which is in agreement with the CV graphs (Figure 2).

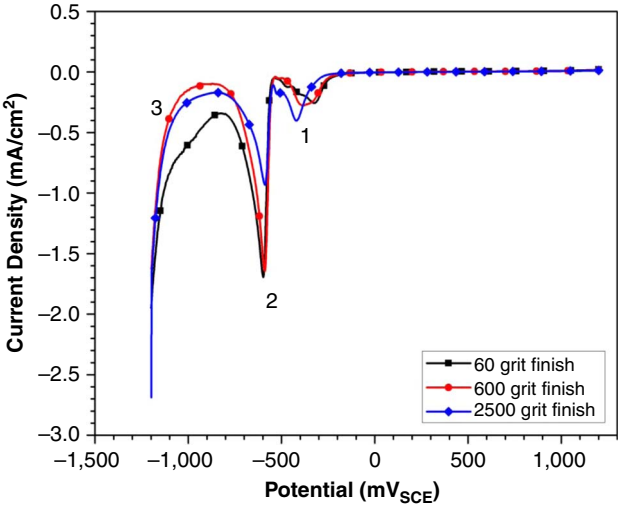

FIGURE 3. *LSVs of the lead alloy electrodes with different surface roughness. The graphs were obtained by linear polarization of the electrode in cathodic direction at 120 mV/min in 4.8 M H_2SO_4 at 25°C. Before LSV the oxide film was grown at constant potential of 1,200 mV_{SCE} for 60 min. The current density was obtained by considering the normalized surface area for each sample determined from BET analysis.*

It was shown in previous studies that the formation of a high-impedance film, i.e., PbO, over the grid during the discharge of the battery, which is also known as grid growth, is the main reason for premature capacity loss.[1-2] Any factor that hinders the formation of this insulating film enhances the battery lifetime. Some alloying elements, such as Sn and Ba, showed practical benefits in reducing the grid growth.[9,11] Moreover, the reduction of this anodic oxide layer to Pb is of importance.[14] The results obtained from the LSV experiments revealed that the stability of oxides on Pb alloys is related to the electrode surface roughness. As can be seen from Figure 3, the reduction of Pb^{2+} to Pb took place at less negative potentials on electrodes with higher surface roughness, which implies a higher stability of the oxide layer on these electrodes. In other words, by increasing the surface roughness, the reduction of Pb^{2+} to Pb occurred at less negative potentials.

Galvanostatic Polarization

Figure 4 shows the galvanostatic anodic polarization curves of a lead electrode in 4.8 M H_2SO_4 solution with different applied current densities. In this method, currents of 2, 5, 10, and 15 mA were applied to the specimens. According to the potentiodynamic polarization diagrams, shown in Figure 1, one may distinguish the potential of the electrode in two regions: an active dissolution area with the corresponding potential of about –500 mV_{SCE} and the oxygen evolution area at the potentials around 2,000 mV_{SCE}. Similarly, three regions can be observed in the galvanostatic diagram. The first region is related to the active dissolution of the lead electrode at the potentials of about –500 mV_{SCE}, which is followed by a rapid increase of the potential to the oxygen evolution area. This increase is arrested at a specific point (depending on applied current and surface roughness) and then the potential decreases slowly, which delineates the second region. Finally, in the third region, the potential reaches a steady-state condition. In this region, many bubbles were formed on the surface of the electrode, implying the evolution of oxygen at these high potentials.

As can be seen from the galvanostatic diagrams, with increasing current the transition from the active dissolution area to the transpassive region took place at shorter polarization times. It should be noted that a rapid increase of the potential from the active dissolution area to the transpassive region might be the result of the formation of the PbO_2 on the surface. After the formation of this oxide on the surface, the potential was high enough that the oxygen evolution reaction occurred. The slow decrease of the potential after the arrest point may be attributed to an increase in the electrochemically active area with the formation of the PbO_2 layer from $PbSO_4$.[13,35] The galvanostatic diagrams show that at a constant current, the rougher the surface, the slower the transit from the active dissolution to the oxygen evolution region. This implies that increasing the surface roughness hindered the passivation, which is in agreement with the potentiodynamic polarization results.

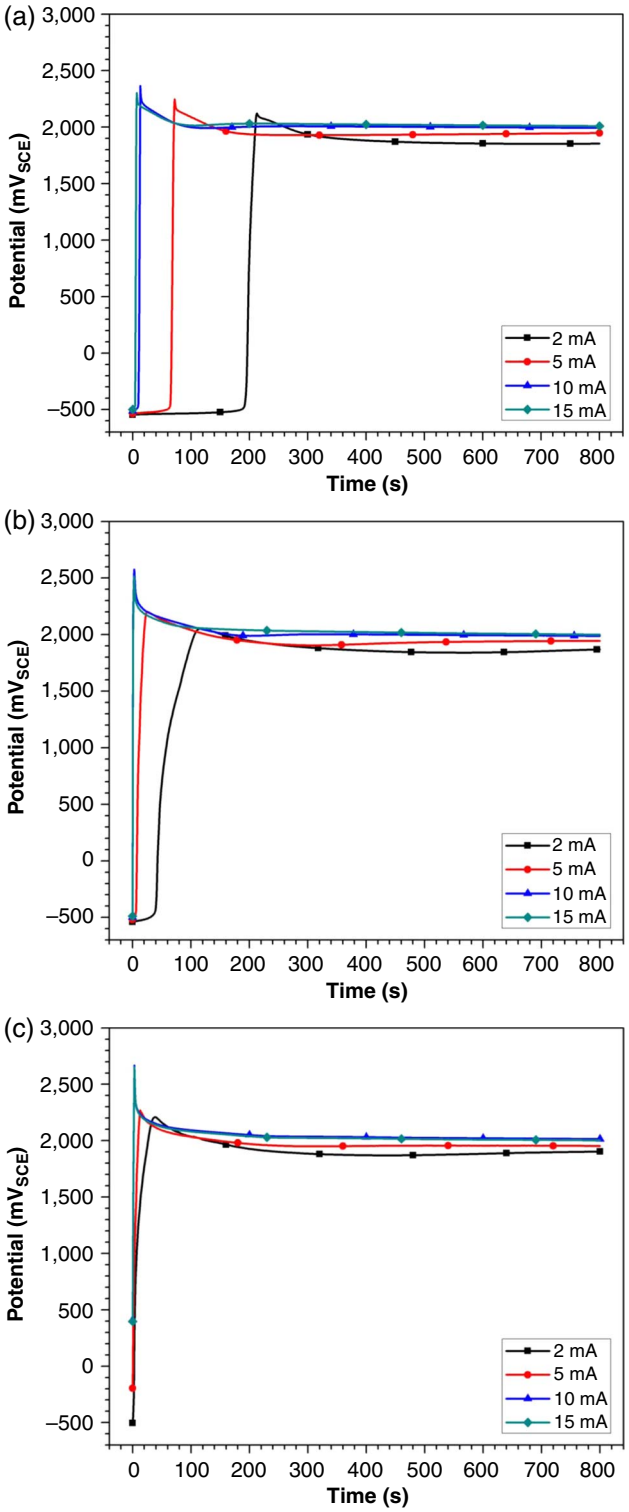

FIGURE 4. *Galvanostatic anodic polarization curves of the lead alloy electrodes with different surface roughness in 4.8 M H_2SO_4 solution at 25°C. (a) 60 grit finish, (b) 600 grit finish, and (c) 2500 grit finish.*

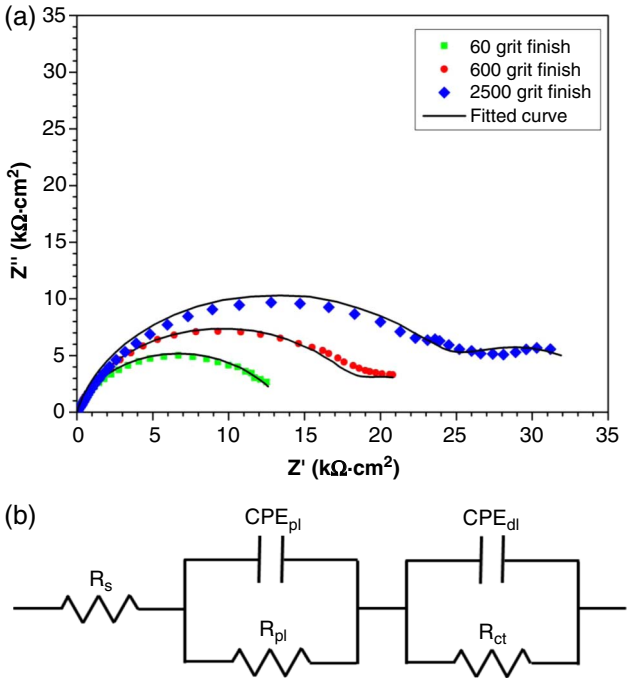

FIGURE 5. *(a) The EIS spectra of the lead alloy electrodes with different surface roughness in 4.8 M H_2SO_4 solution at 25°C. The EIS was conducted at the potential of 1,200 mV_{SCE}. Before impedance measurements the oxide film was grown at constant potential of 1,200 mV_{SCE} for 60 min. (b) Proposed equivalent circuit. The impedance was obtained by considering the normalized surface area for each sample determined from BET analysis.*

Electrochemical Impedance Spectroscopy Analysis

The electrochemical impedance spectroscopy (EIS) spectra of the lead alloy electrode in concentrated sulfuric acid solution are shown in Figure 5(a). EIS was conducted at the potential of 1,200 mV_{SCE} in the range of 100 kHz to 10 mHz with an AC voltage signal with the amplitude of 10 mV. Before measuring the impedance, the passive layers were formed potentiostatically at the potential of 1,200 mV_{SCE} for 60 min. Each impedance diagram shows two capacitance characteristics. According to this, the equivalent circuit with two time constants is proposed and shown in Figure 5(b). In this equivalent circuit R_s, R_{pl}, and R_{ct} denote the solution resistance, the passive layer resistance, and the charge transfer resistance, respectively. CPE_{pl} and CPE_{dl} represent the constant phase element (CPE) of the passive layer and the CPE for double layer, respectively. The data were analyzed with the EIS Analyzer† software and the parameters obtained from fitting the spectrum are listed in Table 2. P_{pl} and P_{dl} indicate the CPE coefficient of the passive layer capacitance and charge transfer capacitance, respectively. Parameters n_{pl} and n_{dl} are the CPE exponent of passive layer resistance and charge transfer resistance, respectively. The values of R_{pl} increased and P_{pl} increased with increasing surface roughness. This suggests that the conductivity of the passive layer increased with increasing surface roughness. Generally, the passive layer of the lead alloy electrode at the potentials near 1,200 mV_{SCE} consists of a laminar structure of PbO and $PbSO_4$ compounds.[36] The $PbSO_4$ layer is at the outer surface of the structure and the PbO is located between the lead alloy and $PbSO_4$. While $PbSO_4$ is a porous layer, the PbO compound is a nonconductive layer and hinders the charge transfer from the active material to the current collectors in a battery.[20] The lower passive layer resistance for the 60 grit finish electrode compared with other specimens implies that the passive layer of this electrode has higher conductivity. The values of R_{ct} and P_{dl} reveal the corrosion behavior of the grid: the higher the R_{ct} and the lower the P_{dl}, the less corrosion occurs on the electrode. As listed in Table 2, R_{ct} increased and P_{dl} decreased by increasing the grit number. Therefore, the specimen with the 2500 grit surface finish has the highest corrosion resistance. For industrial usage, a balance must be struck between two opposing factors, i.e., corrosion resistance and oxygen overpotential. This study's results show that the surface finish of the 600 grit electrode is a good compromise.

Mott-Schottky Analysis

In order to assess the semiconductive properties of the oxide films, the electrochemical capacitance was determined. The capacitance of the film/electrolyte interface (C) is a combination of two capacitors in series, i.e., the space-charge capacitance (C_{sc}) and the double-layer capacitance (C_{dl}):

$$\frac{1}{C} = \frac{1}{C_{sc}} + \frac{1}{C_{dl}} \quad (2)$$

The interfacial capacitance is obtained from $C = 1/\omega Z''$, where ω is the angular frequency and Z'' is the imaginary part of the specific impedance. Assuming that the double-layer capacitance is sufficiently high that it can be neglected compared with the space-charge capacitance, the measured capacitance, C, is equal to the space-charge capacitance, C_{sc}. According to the Mott-Schottky theory,[26] the space-charge capacitance of an n-type semiconductor is given by Equation (3):

$$\frac{1}{C^2} = \frac{2}{\varepsilon\varepsilon_0 e N_d}\left(E - E_{fb} - \frac{kT}{e}\right) \quad (3)$$

where ε is the dielectric constant of the oxide, ε_0 is the vacuum permittivity, e is the electron charge, N_d is the donor density for an n-type passive film, E is the applied potential, E_{fb} is the flat band potential, k is the Boltzmann constant, and T is the absolute

† Trade name.

TABLE 2

The Parameters Obtained from the Fitted Curves of the EIS Analysis of Lead Alloy Electrodes with Different Surface Roughness

Grit Number	R_s ($\Omega \cdot cm^2$)	R_{pl} ($\Omega \cdot cm^2$)	P_{pl} ($F/s^{1-n} \cdot cm^2$)	n_{pl}	R_{ct} ($\Omega \cdot cm^2$)	P_{dl} ($F/s^{1-n} \cdot cm^2$)	n_{dl}
60	3	12,577	2.89×10^{-05}	0.84	2,050	0.004	0.80
600	1.8	18,687	1.86×10^{-05}	0.84	5,420	0.002	0.92
2500	3	25,350	1.17×10^{-05}	0.86	9,800	0.001	0.97

temperature. For an n-type semiconductor, C^{-2} vs. E should be linear with a positive slope, which is contrarily proportional to the donor density of the passive oxide film.

Figure 6 shows the Mott-Schottky plots obtained in 4.8 M H_2SO_4 solution at 25°C as a function of surface roughness after passive film growth at 1,200 mV_{SCE} for 60 min. The positive slope of the linear region in Figure 6 clearly shows that the passive film on Pb alloy is an n-type semiconductor, regardless of the surface roughness. The slope of the Mott-Schottky plots, which decreased with increasing the surface roughness, were calculated to be 29.45, 46.10, and 60.50 $cm^4/F^2 \cdot V$ for surface finish of 60, 600, and 2500 grit, respectively. This implies that the surface roughness affects the electronic properties of the passive film. According to Equation (3), the density of defects of the passive film formed on a Pb alloy is directly influenced by surface roughness, i.e., by increasing the surface roughness the donor density of the passive film increased.

For the oxide film formed on the lead alloy at 1,200 mV_{SCE} in sulfuric acid solution, the major component is Pb^{2+} (PbO and $PbSO_4$). PbO is believed to be a p-type semiconductor, as it is an oxide with interstitial

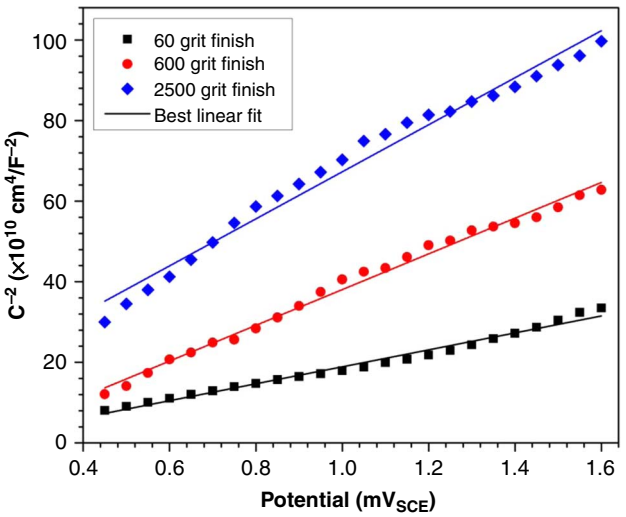

FIGURE 6. *The Mott-Schottky plots of the lead alloy electrodes as a function of surface roughness obtained in 4.8 M H_2SO_4 solution at 25°C after passive film growth at constant potential of 1,200 mV_{SCE} for 60 min. The capacitance was obtained by considering the normalized surface area for each sample determined from BET analysis.*

oxygen.[13] However, Pavlov, et al., has maintained that at low oxygen pressure, PbO has an n-type conductivity whereas at higher pressures, p-type conductivity prevails.[34] By means of EIS analysis, the probability of existence of PbO_2 in the anodic film formed at 1,280 mV_{SCE} has been argued.[37] Moreover, the positive slopes of Mott-Schottky plots (Figure 6), which are in agreement with other research,[13,16] indicate the n-type semiconductive character of the anodic film. Therefore, it is reasonable to consider the passive film formed at the oxidation potential as an n-type semiconductor. Three potential regions during electrochemical oxidation of the Pb electrode in H_2SO_4 solution were reported.[38] Upon oxidation of Pb from –1,410 mV_{SCE} to –840 mV_{SCE}, the anodic layer comprises $PbSO_4$ crystals. The $Pb/PbO/PbSO_4$ electrode system is formed when a lead electrode is immersed in H_2SO_4 solution and polarized within the potential range from –40 mV_{SCE} to 510 mV_{SCE} (equal to 400 mV to 950 mV vs. Hg/Hg_2SO_4).[19] Using electrochemical and photoelectrochemical techniques it has been shown that, at potentials more positive than 510 mV_{SCE}, the PbO layer is oxidized to a non-stoichiometric oxide PbO_n (where $1 < n < 2$).[34] By further oxidation, α-PbO_2 nucleation takes place. Combined x-ray diffraction with chemical analysis has shown that PbO_2 forms at potentials more positive than 1,410 mV_{SCE}.[28,36] Therefore, there is a strong possibility that the n-type character of the passive film formed at 1,200 mV_{SCE} on the Pb alloy is a result of the existence of non-stoichiometric oxide within the film.

There are several factors influencing the electronic properties of the passive film formed on the lead alloys. In the presence of alloying elements the oxidation process alters, as the dopants affect not only the semiconducting properties of the oxide film, but also the mobility of ionic defects.[20] In tetraborate solution, the conductivity of the passive films of Pb-Sn alloys is related to a noticeable enrichment of tin oxide. However, in the presence of sulfuric acid, the ionic conductivity of passive oxide film increases by dissolution of tin oxide.[5] Also, the electrode temperature influences the donor behavior of the lead oxide film. The higher the temperature, the lower the density of defects in the oxide film.[16] Using combined photoelectrochemistry and EIS techniques, Bojinov, et al.,[39] found that tin catalyzes the oxidation of Pb^{2+} to Pb^{4+}, which increases the amount of non-stoichiometric oxide, and facilitates the formation of a highly conductive corrosion

layer, i.e., PbO_2, on lead alloys. Besides all of these factors, i.e., chemical composition of the alloy, applied potential, and temperature, the results of the present study clearly show that the surface roughness of the electrode affects the semiconducting properties of the passive film.

As discussed previously, the plastic deformation increases the crystal defects within the abrasion-induced layer, i.e., vacancies, dislocation density, and sub-grain boundaries. Moreover, it was reported that the donor density of oxide film increases as a result of cold plastic deformation of the bulk alloy.[40] The results of the Mott-Schottky analysis clearly showed that the donor density of the passive film depends on the surface roughness. Therefore, one may conclude that the density of defects within the passive film is proportional to the crystal defects of the surface on which the film was formed. However, further investigations are required to comprehend the relationship between the crystal defects and the passivity of the lead alloys.

CONCLUSIONS

❖ The influence of surface roughness on the electrochemical and passive behavior of a lead-acid battery positive grid alloy was investigated. The oxidation and reduction reactions that occurred on the electrode were facilitated as the surface roughness increased. Moreover, the 600 grit finish specimen had the highest value of overpotential for the oxygen evolution reaction, although the oxygen evolution behavior of the 60 and 2500 grit finish specimens was nearly equal. For the case of the hydrogen evolution overpotential, the 600 and 2500 grit finish specimens were essentially the same, while the specimen with the 60 grit finish surface had a lower overpotential value. The galvanostatic polarization results showed that by increasing the roughness of the electrode surface, the transition time from active dissolution to oxygen evolution increased. The Mott-Schottky analysis revealed that the donor density of the passive film is proportional to the surface roughness.

REFERENCES

1. A.F. Hollenkamp, *J. Power Sources* 59 (1996): p. 87-98.
2. A.F. Hollenkamp, K.K. Constanti, M.J. Koop, L. Apăteanu, M. Calábek, K. Micka, *J. Power Sources* 48 (1994): p. 195-215.
3. P. Ruetschi, *J. Power Sources* 127 (2004): p. 33-44.
4. B. Culpin, A.F. Hollenkamp, D.A.J. Rand, *J. Power Sources* 38 (1992): p. 63-74.
5. P. Simon, N. Bui, F. Dabosi, *J. Power Sources* 50 (1994): p. 141-152.
6. J. Furukawa, Y. Nehyo, S. Shiga, *J. Power Sources* 133 (2004): p. 25-31.
7. S. Fouache, A. Chabrol, G. Fossati, M. Bassini, M. Sainz, L. Atkins, *J. Power Sources* 78 (1999): p. 12-22.
8. D. Slavkov, B.S. Haran, B.N. Popov, F. Fleming, *J. Power Sources* 112 (2002): p. 199-208.
9. L. Albert, A. Goguelin, E. Jullian, *J. Power Sources* 78 (1999): p. 23-29.
10. P. Hosseini Benhangi, D. Nakhaie, M.H. Moayed, A. Molazemi, *J. Power Sources* 196 (2011): p. 10424-10429.
11. N. Bui, P. Mattesco, P. Simon, N. Pébère, *J. Power Sources* 73 (1998): p. 30-35.
12. H.-T. Liu, J. Yang, H.-H. Liang, J.-H. Zhuang, W.-F. Zhou, *J. Power Sources* 93 (2001): p. 230-233.
13. D.G. Li, J.D. Wang, D.R. Chen, *J. Power Sources* 235 (2013): p. 202-213.
14. H.Y. Chen, S. Li, A.J. Li, D. Shu, W.S. Li, C.L. Dou, Q. Wang, G.M. Xiao, S.G. Peng, S. Chen, W. Zhang, H. Wang, *J. Power Sources* 168 (2007): p. 79-89.
15. D. Nakhaie, P.H. Benhangi, A. Alfantazi, A. Davoodi, *Electrochim. Acta* 115 (2014): p. 189-196.
16. D.G. Li, D.R. Chen, J.D. Wang, H.S. Chen, *J. Power Sources* 196 (2011): p. 8789-8801.
17. N. Bui, P. Mattesco, P. Simon, J. Steinmetz, E. Rocca, *J. Power Sources* 67 (1997): p. 61-67.
18. D.A. Rand, D. Boden, C. Lakshmi, R. Nelson, R. Prengaman, *J. Power Sources* 107 (2002): p. 280-300.
19. D. Pavlov, *Lead-Acid Batteries: Science and Technology: A Handbook of Lead-Acid Battery Technology and Its Influence on the Product* (Amsterdam, The Netherlands: Elsevier Science Ltd., 2011).
20. R.D. Prengaman, *J. Power Sources* 95 (2001): p. 224-233.
21. M.H. Moayed, N.J. Laycock, R.C. Newman, *Corros. Sci.* 45 (2003): p. 1203-1216.
22. T. Hong, M. Nagumo, *Corros. Sci.* 39 (1997): p. 1665-1672.
23. G.T. Burstein, P.C. Pistorius, *Corrosion* 51 (1995): p. 380-385.
24. S.-S. Wang, J.-T. Jiang, S.-L. Dai, D.N. Seidman, G.S. Frankel, L. Zhen, *J. Electrochem. Soc.* 161 (2014): p. C433-C440.
25. R. Walter, M.B. Kannan, *Mater. Des.* 32 (2011): p. 2350-2354.
26. S. Ahn, H. Kwon, D.D. Macdonald, *J. Electrochem. Soc.* 152 (2005): p. B482-B490.
27. S. Zhong, J. Wang, H.K. Liu, S.X. Dou, M. Skyllas-Kazacos, *J. Power Sources* 66 (1997): p. 107-113.
28. D. Pavlov, N. Iordanov, *J. Electrochem. Soc.* 117 (1970): p. 1103-1109.
29. S.-S. Wang, G.S. Frankel, J.-T. Jiang, J.-F. Chen, S.-L. Dai, L. Zhen, *J. Electrochem. Soc.* 160 (2013): p. C493-C502.
30. R. Babić, M. Metikoš-Huković, N. Lajqy, S. Brinić, *J. Power Sources* 52 (1994): p. 17-24.
31. S. Brinić, M. Metikoš-Huković, R. Babic, *J. Power Sources* 55 (1995): p. 19-24.
32. T. Hirasawa, K. Sasaki, M. Taguchi, H. Kaneko, *J. Power Sources* 85 (2000): p. 44-48.
33. I. Petersson, E. Ahlberg, *J. Power Sources* 91 (2000): p. 137-142.
34. D. Pavlov, C.N. Poulieff, E. Klaja, N. Iordanov, *J. Electrochem. Soc.* 116 (1969): p. 316-319.
35. J.Z. Liang, H.Y. Chen, M.C. Tang, Y.M. Wu, G.M. Xiao, H.W. Zhou, W.S. Li, X. Jiang, *J. Power Sources* 158 (2006): p. 908-913.
36. E.E. Abd El Aal, *J. Power Sources* 75 (1998): p. 36-43.
37. D. Pavlov, *J. Electroanal. Chem. Interfacial Electrochem.* 118 (1981): p. 167-185.
38. D.G. Li, J.D. Wang, D.R. Chen, *J. Power Sources* 210 (2012): p. 163-171.
39. M. Bojinov, K. Salmi, G. Sundholm, *Electrochim. Acta* 39 (1994): p. 719-726.
40. D. Nakhaie, A. Davoodi, G.R. Ebrahimi, *Corrosion* 72 (2016): p. 110-118.